Journal of Materials Chemistry B

ROYAL SOCIETY OF CHEMISTRY

PAPER

View Article Online
View Journal | View Issue

Cite this: J. Mater. Chem. B, 2025, 13, 7155

A dual-functional biodegradable composite coating fabricated on sulfonated PEEK *via* vacuum cold spraying: immunomodulation-driven osteointegration

Rui Ma, †[a] Zidong Wu,†[a] Xiaoyu Guo,[a] Zixuan Wu,[a] Zheyue Zhu,[a] Yuning Qu,[a] Kunzheng Wang,[a] Chengxin Li,[b] Kai Ma*[b] and Pei Yang*[a]

Received 19th March 2025,
Accepted 12th May 2025

DOI: 10.1039/d5tb00628g

rsc.li/materials-b

Polyetheretherketone (PEEK) is a promising orthopedic implant alternative to metals due to its bone-mimetic modulus and biocompatibility; yet, its bioinert nature often triggers fibrous encapsulation and impedes osteointegration. Here, a biodegradable calcium silicate/β-tricalcium phosphate (CS/TCP) composite coating was fabricated on sulfonated PEEK (SP) *via* vacuum cold spraying to address these limitations. The CS/TCP coating exhibited robust bonding strength, enhanced hydrophilicity, and sustained release of Ca/Si ions, fostering apatite deposition in simulated body fluid. This bioactive interface promoted an immunomodulatory microenvironment by polarizing macrophages toward the anti-inflammatory M2 phenotype. Synergistically, ionic release and cytokine secretion enhanced MC3T3-E1 cell adhesion, proliferation, and osteogenic differentiation. *In vivo*, CS/TCP–SP reduced fibrous tissue thickness in a rat air-pouch model and improved bone–implant integration in rabbit cranial defects. The scalable coating strategy transforms inert PEEK into a bioactive, immunoregulatory implant, demonstrating potential to mitigate aseptic loosening and revision surgeries.

1. Introduction

End-stage arthropathy caused by degenerative changes, congenital abnormalities, tumors, or trauma is typically treated by artificial joint replacement in the clinic. Metal-based materials are commonly used in artificial joint prostheses. Their elastic moduli are much greater than those of normal bone tissue, causing a stress-shielding effect that leads to periprosthetic fracture,[1] and they produce wear particles that may cause aseptic loosening.[2]

Polyetheretherketone (PEEK) has an elastic modulus close to that of human bone tissue and is chemically stable and highly biocompatible and highly processable.[3] PEEK has been used in the preparation of spinal interbody fusion devices and fixed anchors for ligament reconstruction. However, PEEK lacks bioactivity and immunomodulation and forms a layer of connective tissues and has low osteointegration efficiency after implantation.[3,4] The adverse macrophage-mediated immune response elicited by the PEEK surface is responsible for the formation of fibrous encapsulation, resulting in inferior osteointegration.[5] Therefore, PEEK must be modified to increase its bioactivity, immunomodulation and osteointegration.

Surface coating has no negative effect on the mechanical properties of PEEK, and coating with bioactive materials can significantly improve the bioactivity of PEEK; however, the stability of the coating should be considered. Many coating techniques have been used in the preparation of surface coatings on PEEK, including radio frequency magnetron sputtering, spin coating technique, aerosol deposition, ionic plasma deposition, plasma immersion ion implantation deposition, electron beam deposition, vacuum plasma spraying, and arc ion plating.[6,7] However, the bonding strength between the coating material and the PEEK matrix is frequently insufficient, and high temperatures cause thermal degradation of PEEK and phase transition of the coating particles, which alters the effectiveness of the surface coating. There is an urgent need for a technology capable of room-temperature processing to prepare coatings on PEEK surfaces that meet strong adhesion requirements.

Vacuum cold spraying (VCS) is a ceramic coating deposition technique performed at room temperature and relies on the high-speed impact of ultrafine particles to adhere to the substrate surface, forming either dense or porous ceramic coatings.[8] This process directly creates coatings through the

[a] Joint and Foot & Ankle Ward of Orthopedic Center, the Second Affiliated Hospital of Xi'an Jiaotong University, Xi'an 710004, Shanxi, China. E-mail: yangpei@xjtu.edu.cn
[b] State Key Laboratory for Mechanical Behavior of Materials, School of Materials Science and Engineering, Xi'an Jiaotong University, Xi'an 710049, China. E-mail: makai@xjtu.edu.cn
† Rui Ma and Zidong Wu contributed equally to this work.

accumulation of solid particles, offering advantages of a short coating cycle, a large coating area, strong adhesion strength, environmental friendliness, and direct formation.[9,10] Notably, this technique can produce ceramic coatings at room temperature without the need for heating or high-temperature sintering, thereby avoiding thermal degradation of the substrate or the coating materials. It is applicable to a variety of substrates, including metals, ceramics, and plastics, enabling the preparation of both dense and porous coatings.[11] This technique is fully capable of meeting the requirements for dense, wear-resistant, or controlled-release coatings, and its application in the field of orthopedics demonstrates significant potential. To date, only Lee and coworkers have reported a cold spray coating on PEEK, and they coated HA onto the PEEK surface using the cold spray technique and reported that the HA coating was homogeneous and strongly bonded to the PEEK substrate.[12,13] Compared with the uncoated PEEK, the HA coating improved the adhesion and viability of human bone marrow mesenchymal stem cells, increased the expression of osteogenic differentiation markers, and accelerated osteointegration after implantation.[12,13] However, because the HA slightly degraded, two interfaces of HA coating/bone and HA coating/PEEK matrix were present after implantation, and the long-term stability of these interfaces was questionable in Lee's studies. If a degradable coating is established on the PEEK surface to induce new bone to replace the coating, the osteointegration and stability at the bone/PEEK interface could theoretically be enhanced.

Our previous study demonstrated that immersion of PEEK in concentrated sulfuric acid formed a 3D porous structure on PEEK, which was named sulfonated PEEK (SP).[14] A degradable coating may be constructed on the SP surface using VCS technology. The 3D porous structure on the SP surface may make bonding of the coating materials easier and stronger and the new bone tissues can be induced to grow onto the 3D porous structure to enhance the osteointegration at the bone/implant interface.

Calcium silicate (CS) was chosen as the coating material. CS possesses good biocompatibility, bioactivity, and degradability and can promote the adhesion, proliferation, and osteogenic differentiation of osteoblasts *in vitro*, as well as osteointegration *in vivo*.[15,16] CS even has a higher bioactivity than hydroxyapatite (HA) and β-tricalcium phosphate (β-TCP).[17,18] However, the degradation rate of CS is too rapid to sustain its biological effects for a long period.[19] β-TCP also has good bioactivity and certain degradability, and its degradation rate is slower than that of CS.[20] Combining CS and β-TCP can solve the problem of rapid degradation of CS.

Immune cells play a crucial role not only in the inflammation phase but also throughout the bone formation and remodeling phase.[21] Macrophages are regulatory cells involved in bone regeneration in the bone immune microenvironment.[22] Inhibition of inflammation and promotion of bone tissue repair through polarization of pro-inflammatory macrophages (M1) to anti-inflammatory macrophages (M2) have been a hot research topic in recent years.[23] M1 macrophages secrete pro-inflammatory cytokines that exacerbate the inflammatory response and inhibit bone healing, while M2 macrophages secrete osteogenic factors that eliminate the inflammatory response and stimulate the differentiation and mineralization of osteoblast precursors and mesenchymal stem cells (MSCs) to promote bone repair.[24] The temporal regulation of M1 and M2 around the implant and the formation of a conducive microenvironment can promote local bone regeneration and optimize bone immunomodulatory effects, thus promoting the processes of osteogenic differentiation, neovascularization, osteointegration and bone remodeling.[25]

To enhance the bioactivity, immunomodulation and osteointegration of PEEK, we fabricated a 3D porous structure on the PEEK surface using sulfonation treatment and coated the CS/β-TCP composite onto the SP surface. We then investigated the material characteristics, the effects of the material surfaces on osteoblasts and macrophages *in vitro*, the influence of coculturing macrophages and materials on osteogenic differentiation of osteoblasts *in vitro*, and the inflammatory response and osteointegration *in vivo*. We propose a dual-functional coating combining sulfonation-induced 3D porosity and CS/TCP biodegradability to simultaneously address immunomodulation and osteogenesis.

2. Experimental

2.1. Raw materials

PEEK discs with thicknesses of 2 mm and diameters of 15 mm were provided by Professor Jie Wei from the East China University of Science and Technology. Disc samples with diameters of 15 mm were used for the characterization tests, *in vitro* cell tests, and *in vivo* rat air-pouch model, and disc samples with diameters of 8 mm were used for the *in vivo* rabbit cranial defect model. Calcium silicate (99%, ∅ 3 μm) and β-tricalcium phosphate (99%, ∅ 500 nm) powders were purchased from Emperor Nano, Nanjing, China.

2.2. Sulfonation treatment of PEEK

The PEEK samples were immersed and cleaned in acetone, ethanol, and deionized water for 10 min, respectively, followed by ultrasonic cleaning in deionized water three times and drying. The PEEK samples were subsequently immersed in concentrated sulfuric acid (95–98%, Lianyungang Hongxing Chemical Co. Ltd, Lianyungang, China) with magnetic stirring for 5 minutes to form the SP samples. The SP samples were then rinsed three times with deionized water and immersed in acetone in an ultrasonic cleaning chamber for 10 min to remove the residual sulfuric acid. After that, all the samples were ultrasonically cleaned in deionized water for 10 min three times to remove residual acetone and finally dried and stored.

2.3. Preparation of CS and CS/β-TCP coatings

To ensure uniform mixing of the CS/TCP composite powder with a mass ratio of 1 : 1, equal masses of CS and TCP powders were added to a ball mill jar, along with an appropriate amount

Table 1 Deposition parameters of vacuum cold spraying

Parameter	Value	Unit
Gas flow rate	5	L min^{-1}
Chamber pressure	<300	Pa
Distance from nozzle exit to substrate	5	mm
Nozzle traversal speed	2	mm s^{-1}
Gas temperature	Room temperature	°C

of zirconia milling balls. The mixture with ethanol as the dispersing medium was ball-milled for 24 hours on a roller jar mill (GMS5, Changsha Mitr Instrument Equipment Co. Ltd, Changsha, China). The milled slurry was subsequently dried in a vacuum oven for subsequent spraying applications. Both the CS and CS/TCP coatings were prepared at room temperature using a VCS process. The complete details of the equipment used in the VCS system have been described elsewhere,[8,10] and the detailed spraying parameters are listed in Table 1. Nitrogen was used as the acceleration gas to carry the powder particles to the vacuum deposition chamber, where the particles accelerated by the nozzle reached velocities of several hundred meters per second, impacting the substrate to form a coating. All the samples were sterilized with ethylene oxide before the cell and animal tests. The samples were divided into three groups as SP, CS coated SP (CS–SP) and CS/TCP coated SP (CS/TCP–SP).

2.4. Microstructure characterization

The microstructures of the coatings were characterized by scanning electron microscopy (SEM; S-4800, HITACHI, Tokyo, Japan). The SEM observations were performed at an accelerating voltage of 10 kV and a chamber pressure of high vacuum. Both secondary electrons (SE) were used for surface morphology characterization. To analyze the elemental composition across the coating surface, energy-dispersive X-ray spectroscopy (EDS; X-Max, Horiba, Kyoto, Japan) was employed in conjunction with SEM. Atomic force microscopy (AFM) measurements were performed using an atomic force microscope (SPM-9700HT, Shimadzu, Kyoto, Japan). AFM analysis was conducted in tapping mode and a 10 μm × 10 μm area was scanned to evaluate surface roughness, which was quantified using arithmetic mean roughness (R_a) and root mean square roughness (R_q) values extracted from the scanned images using the NanoScope Analysis software. R_a is the arithmetic mean of the absolute values of height deviations relative to the central plane within the observed area. R_q is the root mean square value of the profile deviations from the mean line over the sampling length. The surface hydrophilicity of the coatings was examined with a contact angle measurement system (DSA100S, KRÜSS, Hamburg, Germany) using the sessile drop method. During the test, a 2 μL water droplet was used for contact angle measurements and static contact angle measurements were performed, with advancing and receding angles not recorded. Five measurements were performed at different points on each sample.

Tensile tests were applied to assess the adhesion strength between the coatings and the substrate. The test was conducted at a stretching rate of 0.02 mm s^{-1}. In the tensile test, epoxy adhesive (E-7) was used to fix the flat ends of the tensile grips (one end is the gripping end and the other is the flat end) to both sides of the sample. After the epoxy adhesive cured, the gripping ends of the tensile grips were attached to the tensile testing machine (DDL100, China Machine Testing, Changchun, China). After a 24-hour curing period, the test was conducted at a tensile rate of 0.02 mm s^{-1}, and the force changes were recorded using a sensor. The experiment was terminated when the sample fractured, and the maximum force at the moment of fracture was used to calculate the fracture strength.

2.5. Ion release tests

All samples were immersed in a Tris–HCl buffer solution at pH 7.4 and incubated at 37 °C. Two-milliliter buffer solution samples were collected at 1, 4, 7, 14, 21 and 28 days, respectively, and the concentrations of Ca and Si ions in the buffer solution samples were detected by inductively coupled plasma atomic emission spectroscopy (ICP-AES; Varian, Palo Alto, USA).

2.6. *In vitro* bioactivity study

The samples in each group were immersed in simulated body fluid (SBF; Solarbio Biotechnology Co., Ltd, Beijing, China) at 37 °C. After 28 days, the samples were removed, cleaned and dried. SEM was used to observe apatite formation on the material surfaces, and EDS was used to analyze the surface chemical composition of the apatite-like materials.

2.7. *In vitro* cell tests of osteoblasts

2.7.1. Cell culture of MC3T3-E1 cells. MC3T3-E1 cells were chosen for the *in vitro* cell tests of osteoblasts. The cells were cultured with Dulbecco's modified Eagle's medium (DMEM; HyClone, Thermo Fisher Scientific Inc., Waltham, USA) supplemented with 10% FBS (100 U mL^{-1}; GibcoBRL, GrandIsland, USA) and 1% penicillin–streptomycin solution (100 U mL^{-1}; GibcoBRL, GrandIsland, USA). The cells were cultured in a humidified incubator at 37 °C with 5% CO_2 and 95% air. The medium was changed every three days.

2.7.2. Cell adhesion and cell proliferation. MC3T3-E1 cells were seeded at a density of 6 × 10^4 cm^{-2} into 24-well plates (Costar, Corning Incorporated, New York, USA) with samples placed beforehand. After 12 and 24 hours of culture, the unadhered cells were rinsed with PBS, and a CCK-8 assay was used to assess the cell adhesion on the material surface. The samples were removed and gently washed three times with phosphate-buffered saline (PBS; pH = 7.4) to remove the unadhered cells and then transferred to a new 24-well plate, after which 50 μL of CCK-8 solution (Dojindo Molecular Technologies Inc., Kumamoto, Japan) was added and the mixture was incubated in an incubator. After incubation for 3 hours, 100 μL of liquid was extracted from each well and transferred to a 96-well plate. The optical density (OD) at 450 nm was read with a microplate reader (Synergy HT, Biotek, Winooski, USA), with 620 nm as the reference wavelength. The relative cell

viability (%) was calculated as follows: [(OD of the experimental group − OD of the blank control group (DMEM)/OD of the tissue culture polysterene (TCPS)] × 100.

MC3T3-E1 cells were seeded on the surface of the samples at a density of 2×10^4 cm^{-2}, and after 1, 3, and 7 days of culture, the CCK-8 assay was used to assess cell proliferation. The specific experimental process was the same as that used for the cell adhesion test.

2.7.3. Cell morphology and cell spreading. MC3T3-E1 cells were seeded at a density of 6×10^4 cm^{-2} into 24-well plates in which each group of samples was placed beforehand. After 24 hours of culture, the unadhered cells were rinsed with PBS. The cells were fixed with 4% paraformaldehyde and stained with rhodamine–phalloidin (5 U mL^{-1}, Biotium, Hayward, USA), and the nuclei were stained with 4′,6-diamidino-2-phenylindole (DAPI; Sigma-Aldrich, St. Louis, USA) to visualize the cells. The spreading of the cytoskeleton on the material surfaces was observed by confocal laser scanning microscopy (CLSM; TCS SP2, Leica, Heidelberg, Germany).

MC3T3-E1 cells were seeded on the sample surfaces at a density of 6×10^4 cm^{-2} and then incubated for 24 hours. The cells were fixed with 2.5% glutaraldehyde, followed by gradient dehydration with alcohol, alcohol replacement with hexamethyldisilazane (HMDS; Sigma-Aldrich, St. Louis, USA), gold spraying, and observation of cell morphology and spreading on the material surfaces by SEM (S-4800, HITACHI, Tokyo, Japan).

2.7.4. Alkaline phosphatase (ALP) staining and quantitative ALP activity assay. MC3T3-E1 cells were cultured with DMEM for 24 hours, and then the medium was changed to osteogenic induction medium containing dexamethasone (100 nM), ascorbic acid (50 μg mL^{-1}) and β-phosphoglycerol (10 mM), which was replaced every three days. After 7 and 14 days of culture, the MC3T3-E1 cells on the material surfaces were stained with an ALP staining kit (Shanghai Renbao, Shanghai, China), in accordance with the instructions provided by the supplier. The cells on the material surfaces were fixed with 4% paraformaldehyde for 30 minutes, after which the samples were stained with the ALP staining kit. After 1 hour, the sample surfaces were washed with PBS to terminate the staining, followed by drying, observation and photographing. The MC3T3-E1 cells cultured on the material surfaces for 7 and 14 days were subjected to ALP quantification using an ALP quantification kit (Nanjing Jiancheng Bioengineering Institute, Nanjing, China) according to the provided protocol. The ODs were measured at 405 nm using a microplate reader (Synergy HT, Bio-Tek, Winooski, USA). Furthermore, the total protein content was determined using a BCA protein assay kit (Pierce, Thermo, Rockford, USA) according to the manufacturer's protocol. Finally, the ALP activity was normalized to the corresponding total protein content.

2.7.5. Alizarin red staining and quantitative analysis. MC3T3-E1 cells on the material surfaces were cultured in osteogenic induction medium. After 21 days of culture, the cells were fixed with 4% paraformaldehyde for 30 minutes, and alizarin red staining solution (pH = 4.20; Sigma-Aldrich, St. Louis, USA) was added after being rinsed with PBS. The cells were stained for 30 minutes at room temperature, and the excess staining solution was removed by washing with the distilled water. Finally, the samples were photographed and observed. The stained samples were immersed in a 10% cetylpyridinium chloride solution (pH = 7.0; Sigma-Aldrich, St. Louis, USA) to elute the staining solution. The optical density of the solution was then measured at 570 nm using a microplate reader (Synergy HT, Bio-Tek, Winooski, USA) to quantify the mineralization of the cells on the material surfaces.

2.7.6. Expression of osteogenic differentiation-related genes. The expression levels of osteogenic differentiation-related genes, including ALP, collagen I (COL I), osteocalcin (OCN), and osteopontin (OPN), were analyzed by a real-time quantitative PCR (RT-qPCR) at 7, 14 and 21 days after being cultured in the osteogenic induction medium. Total mRNA was extracted using the TRIzol reagent (Ambion, GrandIsland, USA) and then reverse transcription to cDNA was performed using a reverse transcription kit (Fermentas, Thermo Scientific Molecular Biology, Pittsburgh, USA). RT-qPCR was performed using LightCycler 480II and LightCycler 480 SYBR Green I Master Mix kits (TaKaRa Biotechnology Co., Dalian, China). The expression gene levels were normalized to those of the SP to compare differences among different groups. The primers used for each gene are shown in Table 2.

2.8. *In vitro* osteoimmunomodulatory properties

2.8.1. Cell culture of RAW264.7 cells. RAW264.7 cells were selected as the cell strain for the *in vitro* macrophage tests. The specific culture method was the same as that used for the MC3T3-E1 cells.

2.8.2. Cell adhesion and cell proliferation. RAW264.7 cells were seeded on the material surfaces at a density of 6×10^4 cm^{-2} in 24-well plates. After 6, 12 and 24 hours of culture, cell adhesion was assessed by the CCK-8 method. The cell density was 2×10^4 cm^{-2} and the time points were 1, 3 and 7 days in the cell proliferation test.

2.8.3. Cell morphology. The cells were cultured on the materials for 24 hours. The samples were subsequently fixed with 2.5% glutaraldehyde, followed by gradient dehydration

Table 2 Primers of osteogenic differentiation-related genes used in the real-time PCR tests

Target gene	Primer sequence (5′ → 3′)
ALP	F: GGGACTGGTACTCGGACAAT R: GGGACTGGTACTCGGACAAT
COL I	F: GGGACTGGTACTCGGACAAT R: GCAGCTGACTTCAGGGATGT
OCN	F: GGTGCAGACCTAGCAGACACCA R: AGGTAGCGCCGGAGTCTATTCA
OPN	F: GCAGCTGACTTCAGGGATGT R: GTGTGCTGGCAGTGAAGGACTC
GAPDH	F: GAGACCTTCAACACCCCAGC R: ATGTCACGCACGATTTCCC

with alcohol, alcohol replacement with hexamethyldisilazane (HMDS, Sigma-Aldrich, St. Louis, USA), gold spraying, and observation of the cell morphology and spreading by SEM (S-4800, HITACHI, Tokyo, Japan).

2.8.4. Immunofluorescence analysis. The polarization of RAW264.7 cells was evaluated by immunofluorescence staining to observe the M1 macrophage marker (iNOS) and M2 macrophage marker (CD206) at 4 days. For immunofluorescence staining, RAW264.7 cells on each sample were permeabilized in 0.1% Triton X-100 for 20 min and blocked with 5% BSA for 60 min at room temperature. The samples were then incubated with primary antibodies including rabbit anti-CD206 (1 : 400; Affinity Biosciences Cat# DF4149, Cincinnati, USA) or rabbit anti-iNOS (1 : 400; Affinity Biosciences Cat# AF0199, Cincinnati, USA) at 4 °C overnight. Secondary antibodies against donkey anti-rabbit 647 (1 : 400; SA00014-7, Proteintech, Chicago, USA) were incubated with the samples for 150 min at room temperature in the dark. After the samples were fully rinsed with PBS, the nuclei were stained with DAPI for 5 min. Finally, the immunofluorescence images of the samples were recorded on a CLSM (A1, Nikon, Tokyo, Japan) and analyzed with ImageJ (1.54f, National Institutes of Health, USA).

2.8.5. Expression of inflammatory cytokines. The interleukin-6 (IL-6), interleukin-1β (IL-1β), inducible nitric oxide synthase (iNOS) and tumor necrosis factor-α (TNF-α) cytokines in the cell culture supernatants were quantitatively detected using ELISA kits (R&D Systems, Lake Bluff, USA). RAW264.7 cells were cultured on the material surfaces for 3 days. The medium was then collected and the supernatant was centrifuged at 300 × *g* for 10 min. The contents of the abovementioned cytokines were assayed according to the instructions for the ELISA kits.

2.9. Osteogenic differentiation of MC3T3-E1 in the macrophage conditioned medium

2.9.1. Preparation of the macrophage-conditioned medium. RAW264.7 cells were seeded on each group of materials and cocultured in 24-well plates, and MC3T3-E1 cells were added to another 24-well plate for culture. After a 48-hour incubation period, the supernatant from each group was harvested from the RAW264.7-culture plates on a daily basis. The harvested supernatant was then combined with 100 nM dexamethasone, 50 μg mL^{-1} ascorbic acid, and 10 mM sodium β-glycerophosphate to generate macrophage-conditioned medium (MCM). The MCM was added to the MC3T3-E1 cells for culture, and the MCM was changed every other day.

2.9.2. ALP staining and quantitative ALP activity assay under conditioned culture. Following incubation of MC3T3-E1 cells in the MCM for 14 days, the MC3T3-E1 cells on the material surfaces were stained using an ALP staining kit (Shanghai Renbao, Shanghai, China), and the ALP activity of the MC3T3-E1 cells was quantitatively analyzed using an ALP quantification kit (Nanjing Jiancheng Bioengineering Institute, Nanjing, China).

2.9.3. Alizarin red staining and quantitative analysis under conditioned culture. MC3T3-E1 cells were cultured in the MCM for 21 days and subsequently stained with alizarin red staining solution (pH = 4.20; Sigma-Aldrich, St. Louis, USA). The stained samples were immersed in a 10% cetylpyridinium chloride solution (pH = 7.0; Sigma-Aldrich, St. Louis, USA) to elute the staining solution. The optical density of the suspension was then measured at 570 nm using a microplate reader (Synergy HT, Bio-Tek, Winooski, USA).

2.9.4. Expression of osteogenic differentiation-related genes under conditioned culture. After MC3T3-E1 cells were cultured with the MCM for 7, 14 and 21 days, the expression levels of osteogenic differentiation-related genes, including ALP, COL I, OCN, and OPN, were analyzed by RT-qPCR. The specific experimental methods were the same as before. The expression gene levels were normalized to those of the SP to compare differences among different groups. The primers used for each gene are shown in Table 2.

2.10. Immunomodulatory evaluation after subcutaneous implantation

A total of 12 male Sprague-Dawley rats (weighing 200 g) were equally divided into three groups (SP, CS–SP and CS/TCP–SP) to establish a rat air-pouch model. The operative procedures and animal care were performed according to the principles of the Second Affiliated Hospital of Xi'an Jiaotong University on animal experimentation. Ethical approval for undertaking the animal experiment was obtained from the institutional ethics board of Xi'an Jiaotong University Health Science Center. The specific modeling method was as follows: on day 1, 10 mL of sterile air was injected subcutaneously into each rat back to form a subcutaneous air-pouch. At days 3 and 6, an additional 5 mL of air was injected to maintain the air-pouch. On day 7, no inflammatory reaction at the injection site or around the air-pouch and the formation of a subcutaneous pouch around the injection site were considered successful. The rats were anesthetized with a 1% pentobarbital sodium solution (1 mL/100 g), and the skin around the air-pouch was prepared and disinfected. The samples in each group were implanted into the subcutaneous air-pouch. Following a seven-day period of implantation, the implant and its surrounding tissue were removed together and placed in 4% paraformaldehyde. The fixed samples were embedded in methyl methacrylate (MMA). After satisfactory curing, the embedding block was removed and securely fixed on the microtome, ensuring that the blade cuts parallel to the surface of the implanted material. The samples were cut along the horizontal plane with a slice thickness of approximately 150 μm. An adhesive was used to bond the slices to acrylic glass slides and the slices were pressed for 24 hours. The hard tissue slices were manually ground using P300, P800, and P1200 sandpaper until the thickness was reduced to 50 μm. Finally, the slices were polished with a polishing cloth and polishing powder to achieve a thickness of 20–30 μm. Finally, the slices were stained with HE staining and were observed with an optical microscope (Olympus CX43, Japan) to assess the formation of connective tissues around the implant. The quantitative analysis of the thickness of the peri-implant connective tissues

was performed using ImageJ software (1.54f, National Institutes of Health, USA).

2.11. Osseointegration evaluation after cranial implantation

A total of 12 female rabbits were equally divided into three groups: SP, CS–SP, and CS/TCP–SP. The rabbits were anesthetized by intravenous injection of 2% sodium pentobarbital (30.0 mg kg^{-1}) at the ear margins. After skin preparation and disinfection, an incision was made along the middle cranial suture, and the tissues were separated layer by layer to expose the parietal bone. A nonpenetrating cylindrical bone defect with a diameter of 8 mm was prepared on each side of the parietal bone using a ball drill while preserving the inner plate barrier. The materials were implanted into the bone defects so that the coated surface adhered to the residual bone. The periosteum and muscle were sutured to cover the materials and then the skin was sutured. Penicillin was administered intraperitoneally for three days following surgery to prevent infection. After 6 weeks, the rabbits were euthanized and the parietal bones with the specimens were removed and placed in 4% paraformaldehyde. Micro-CT scanning (AX-2000, Aoying Inspection Technology Co., Ningbo, Zhejiang) was conducted, and a 200 μm region surrounding the implant was selected as the region of interest (ROI) for reconstruction (VG Studio MAX 3.5, Heidelberg, Germany). Four parameters were analyzed using CTAn software (SkyScan, Belgium), including bone volume/total volume (BV/TV), trabecular bone number (Tb·N), trabecular bone thickness (Tb·Th) and trabecular bone separation (Tb·Sp). The specimens were subsequently embedded in methyl methacrylate (MMA), processed for hard tissue sectioning, and finally Goldner stained and observed with an optical microscope (Olympus CX43, Japan).

2.12. Statistical analysis

All the quantitative data are presented as mean ± standard deviation. All the experiments were repeated at least three times. The data were subjected to statistical analysis using two-way analysis of variance (ANOVA) for comparative analysis, and the comparisons between each pair of groups were made using the least significant difference (LSD) method. A $p < 0.05$ was considered to indicate a significant difference. All the data were analyzed using SPSS software (IBM SPSS Statistics 19, USA).

3. Results and discussion

3.1. Materials characterization

Sulfonation treatment is a commonly used surface modification technique for PEEK to create a porous surface topography.[26] In this study, a 3D porous mesh structure was formed on a PEEK surface after being treated with concentrated sulfuric acid according to SEM observations (Fig. 1A1 and A4). This might enhance the adhesion of sprayed particles and promote cell attachment and proliferation. The EDS spectrum revealed that only C and O peaks were present, and the low peak of S indicated a small amount of sulfuric acid residue. According to the results of our previous studies, the residual concentrated sulfuric acid on the surface of SP can be mostly removed by acetone immersion without affecting the cytocompatibility of the material.[14] Therefore, the remaining sulfuric acid on the SP surface was negligible. Many uniformly distributed particles with diameters of hundreds of nanometers to several micrometers were deposited on the CS–SP and CS/TCP–SP surfaces. EDS showed that distinct Ca and P elemental peaks were present on the surface of CS–SP (Fig. 1A8), demonstrating the presence of CS; and distinct Ca, P and Si elemental peaks were present on the surface of CS/TCP–SP (Fig. 1A9), demonstrating the presence of CS and TCP.

In vivo, all bioactive materials form a bone-like apatite layer on their surfaces and bind to bone through this apatite layer.[27] The *in vitro* SBF immersion test represents the gold standard for evaluating the *in vitro* bioactivity of biomaterials.[28] After 14 days of immersion in SBF, numerous apatite-like particles formed on the surface of SP, and dense clustered and lamellar apatite layers formed on the CS–SP and CS/TCP–SP surfaces (Fig. 1B), indicating that both CS–SP and CS/TCP–SP exhibited robust surface bioactivity. In addition, the newly formed substances after immersion in SBF presented peaks of Ca and P (Fig. 1B7–B9), indicating the formation of apatite. It was conceivable that the CS–SP and CS/TCP–SP coatings could induce the deposition of Ca and P ions to form apatite layers *in vivo*, which facilitated the growth of mesenchymal stem cells and osteoblasts as well as subsequent osteointegration. Both CS and β-TCP, especially CS, exhibited excellent bioactivity. We speculated that the mechanism of apatite formation on the surface of CS–SP and CS/TCP–SP was as follows:[29–31] upon contact with SBF, CS released Ca^{2+}, which exchanged with H^+ in SBF to form silanol groups (Si–OH). Negatively charged Si–OH could adsorb Ca^{2+} to deposit onto the surface of CS–SP or CS/TCP–SP by electrostatic adsorption. The accumulation of Ca^{2+} resulted in a positively charge-dominated surface, which could adsorb PO_4^{3-} to deposit onto the material surface to form apatite nuclei. The continuous consumption of Ca and P ions allowed the apatite nuclei to grow and form apatite layers.[32]

As shown in Fig. 2A, PEEK sulfonation followed by vacuum cold spray coating changed the general color of the samples. Based on the above results, the CS and CS/TCP coatings were successfully prepared on the SP surfaces using the vacuum cold spraying technique. The hydrophilicity of the material surface influences the adhesion, proliferation and osteogenic differentiation of the cells.[33,34] The results of the water contact angle measurements demonstrated that the water contact angle of SP was 78 ± 8°, whereas those of CS–SP and CS/TCP–SP were 64 ± 2° and 32 ± 3°, respectively (Fig. 2B). The statistical results indicated that the water contact angle decreased in the order of CS/TCP–SP > CS–SP > SP. The results demonstrated that the CS and CS/TCP coatings enhanced the hydrophilicity of SP, especially the CS/TCP coating. Compared with hydrophobic surfaces, hydrophilic surfaces are more conducive to cell adhesion, spreading and differentiation than the hydrophobic surfaces.[33,35] The topography of the material surfaces was observed and the surface roughness (R_a and R_q) of the material

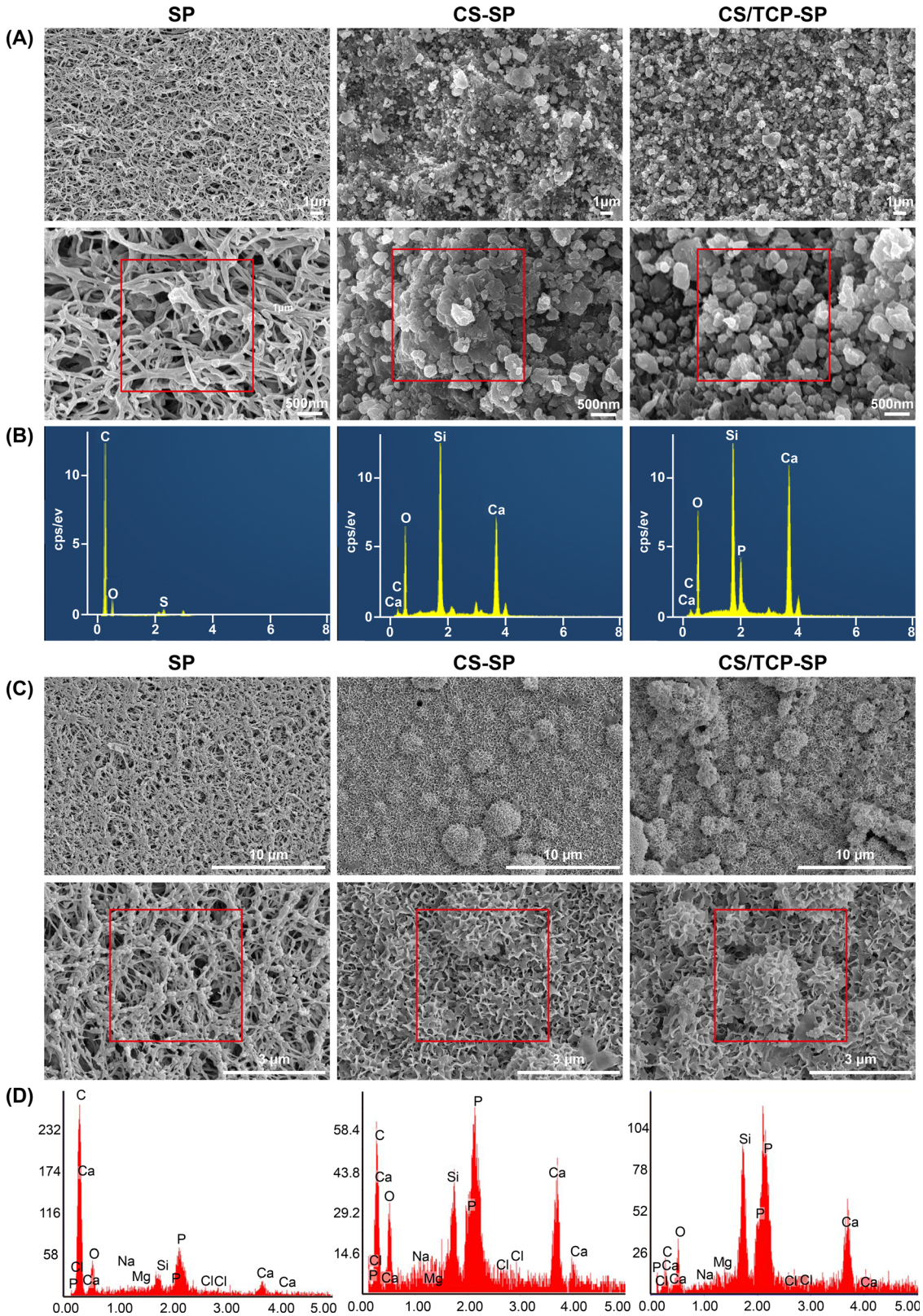

Fig. 1 Surface morphology and chemical composition of the materials before and after SBF immersion: (A) FE-SEM (A1)–(A6) and EDS (A7)–(A9B) before SBF immersion and (B) FE-SEM (B1)–(B6C) and EDS (B7)–(B9D) after SBF immersion.

surfaces was quantified by AFM. The observation of the surface morphology of the material by AFM (Fig. 2C) was in accordance with the SEM results. The CS coating significantly improved the surface roughness of SP, and the R_a and R_q of CS/TCP–SP were

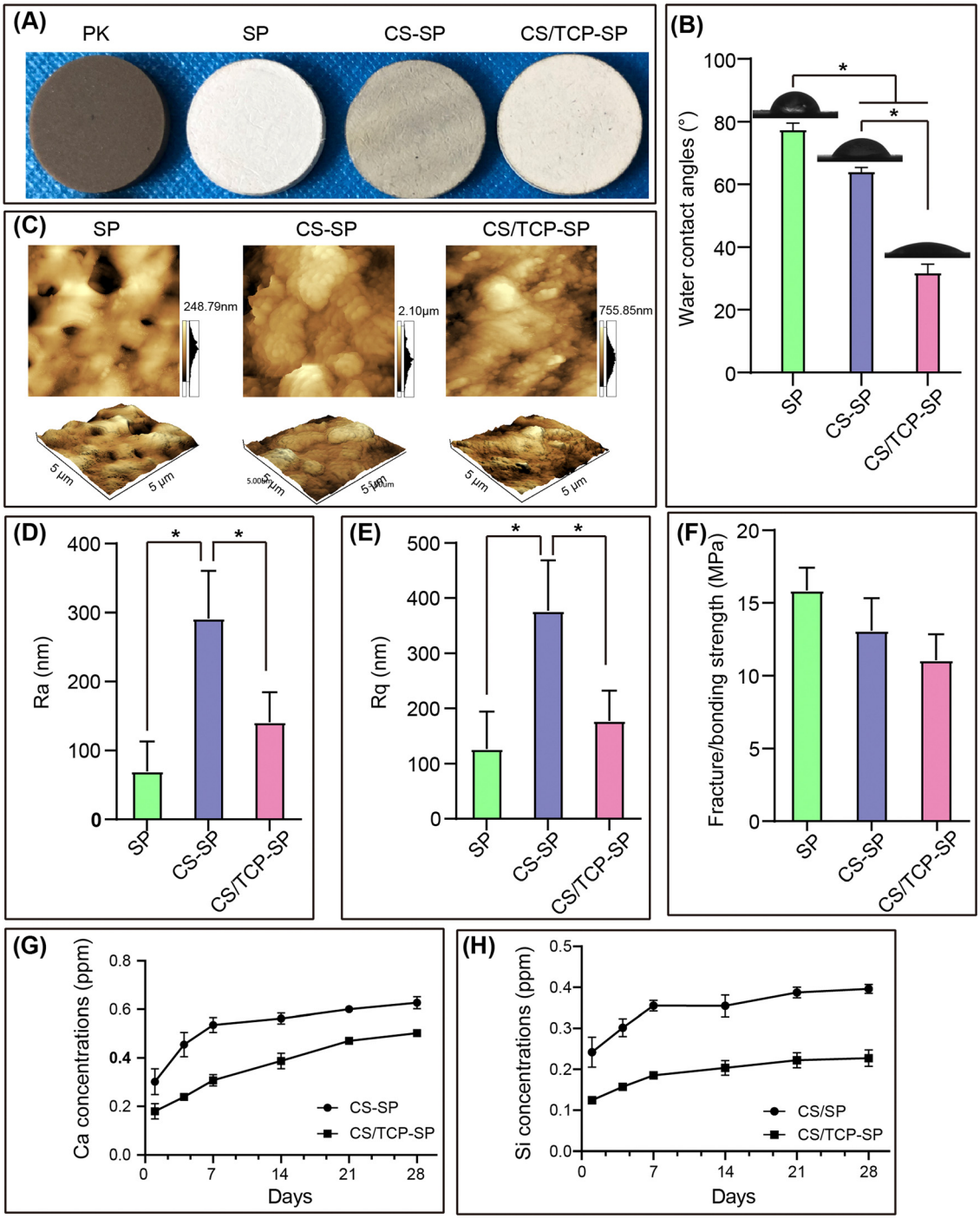

Fig. 2 Material characterization: (A) gross morphology of the materials (PK, SP, CS–SP and CS/TCP–SP); (B) surface hydrophilicity measured by water contact angles; (C) surface topological structures observed by AFM; (D) and (E) surface roughness data (R_a and R_q); (F) fracture/binding strength measured by the tensile tests; and (G) and (H) elemental concentrations of Ca and Si as determined by ICP-OES after SP, CS–SP and CS/TCP–SP immersed in Tris–HCl buffer for different times.

greater than those of SP; however, the differences were not significant (Fig. 2D and E). Furthermore, the surface roughness (R_a and R_q) of CS–SP was considerably greater than that of CS/TCP–SP, which might be attributed to the larger particle size of CS (3 μm) than that of TCP (500 nm).

We measured the bonding strength of the coatings by tensile testing and reported that the sulfonated layer of the SP surface presented a fracture strength of 16 ± 2 MPa, whereas the CS and CS/TCP coatings presented bonding strengths of 13 ± 2 MPa and 11 ± 2 MPa, respectively (Fig. 2F). These results demonstrated that the CS and CS/TCP coatings on the SP surface exhibited a stable bonding with the SP substrate. However, Lee reported a bonding strength of 7.16 MPa for HA coatings on PEEK surfaces prepared by cold spraying.[12]

In contrast, the bonding strength of the CS/TCP–SP coating in this study was significantly greater than that reported in the previous study. Although the spraying principle in this study was the same as that of Lee, the specific equipment and spraying conditions for spraying were markedly disparate. We sprayed the samples in a vacuum environment at room temperature, whereas Lee's team sprayed them in air at high temperature (200, 300, and 400 °C). These differences in spraying conditions might have contributed to the discrepancy in the final bonding strength.

3.2. *In vitro* release of Ca and Si ions

The ion release of the coatings was assessed by measuring the concentrations of Ca and Si ions in the Tris–HCl solution. Fig. 2G and H show that CS–SP released considerable quantities of Ca and Si ions within 7 days, but the release of Ca and Si ions subsequently decreased significantly. The CS/TCP–SP gradually released Ca ions for up to 21 days and Si ions up to 14 days. These results indicated that the CS coating degraded faster than the CS/β-TCP coating within 7 days, whereas the CS/β-TCP composite coating gradually degraded within 14 days. Although the CS coating on the CS–SP surface was bioactive, it degraded faster within 7 days to exert biological effects for a longer time. The addition of TCP to the coating material of CS/TCP–SP was intended to retard the degradation of the coating to preserve the biological effects to a maximum extent.

3.3. *In vitro* biocompatibility of osteoblasts

The interaction between cells and material surfaces is a crucial indicator for evaluating the bioactivity of biomaterials. The adhesion, proliferation and spreading of osteoblasts on material surfaces are necessary for osteointegration between the material surface and bone tissues.[36] We assessed the biocompatibility of the materials by evaluating the adhesion, proliferation, spreading and morphology of MC3T3-E1 cells on the material surfaces. The results of the CCK-8 assays demonstrated that cell adhesion and proliferation were greater at all time points on the surface of CS/TCP–SP than those on the surface of SP. Compared with those on CS–SP and CS/TCP–SP, the number of cells on CS/TCP–SP was consistently greater than that on CS–SP at all time points, and no statistically significant difference was observed between these groups (Fig. 3B and C). As shown in the CLSM images, the CS/SP and CS/TCP–SP groups presented greater numbers of cells, greater spreading efficiencies, larger spreading areas, and greater densities of actin microfilaments connecting neighboring cells than the SP (Fig. 3D). These results indicated that the cell spreading on the CS/SP and CS/TCP–SP surfaces was significantly superior to that on the SP surface. The SEM images of the cells on the material surfaces demonstrated that the cells on the SP surface were dispersed, sparse, and in poor condition. In contrast, the cells on the CS–SP and CS/TCP–SP surfaces were more numerous, distributed over a larger area, and presented a greater number of pseudopods anchored to the material surfaces (Fig. 3E).

Therefore, the coated SP materials (CS–SP and CS/TCP–SP) demonstrated enhanced adhesion, proliferation, and spreading of MC3T3-E1 cells on the surface compared with those of SP. These observed outcomes could be attributed to the increased hydrophilicity and roughness, excellent bioactivity and cytocompatibility of CS and β-TCP, and the release of Ca and Si ions. Favorable cell adhesion, proliferation and spreading facilitate subsequent osteogenic differentiation and osteointegration.

3.4. *In vitro* osteogenic differentiation

Following the adhesion and proliferation stages, osteoblasts on the surface of biomaterials enter the osteogenic differentiation phase to synthesize collagen and a number of other proteins to induce mineralization.[37] The osteogenic differentiation ability of the materials was evaluated by examining the expression of ALP activity, calcium nodule formation, and osteogenic differentiation-related genes (ALP, COL I, OCN and OPN) of MC3T3-E1 cells. As an early marker of osteogenic differentiation, ALP activity was evaluated after MC3T3-E1 cells were cultured for 7 and 14 days. The ALP staining results (Fig. 4A) indicated that the ALP staining became denser and darker from SP to CS–SP and to CS/TCP–SP. A similar trend was observed in the results of the ALP activity quantification (Fig. 4B). The ALP activities of CS–SP and CS/TCP–SP were significantly greater than that of SP at both 7 and 14 days, and the ALP activity of CS/TCP–SP was significantly greater than that of CS–SP. Similarly, alizarin red staining gradually deepened and increased from SP to CS–SP and then to CS/TCP–SP (Fig. 4C). We evaluated the number of calcium nodules by quantitative analysis of the alizarin red staining, and the results demonstrated that the highest number of calcium nodules was observed on the surface of CS/TCP–SP, followed by CS–SP, and the lowest number of calcium nodules was observed on the surface of SP (Fig. 4D). The results of quantitative real-time PCR demonstrated (Fig. 4F) that the expression levels of osteogenic differentiation-related genes appeared to be different at 14 days. The expression levels of ALP, COL I, OCN and OPN on CS–SP and CS/TCP–SP were significantly greater than those on SP, whereas the expression levels of the remaining three groups of genes did not differ between CS–SP and CS/TCP–SP with the exception of the difference in the expression of ALP. At 21 days (Fig. 4G); there were significant differences in the expression levels of osteogenic differentiation-related genes among different groups; the expression levels of ALP, COL I, OCN and OPN on CS–SP and CS/TCP–SP were significantly higher than those on SP, and the expression levels of ALP, COL I, OCN and OPN on CS/TCP–SP were also greater than those on CS–SP.

The coated SP materials (CS–SP and CS/TCP–SP) demonstrated enhanced adhesion, proliferation, spreading, and expression of osteogenic differentiation-related genes of MC3T3-E1 cells compared with those of SP. Compared with CS–SP, CS/TCP–SP demonstrated comparable cell adhesion, proliferation, and spreading. However, CS/TCP–SP exhibited significantly enhanced osteogenic differentiation, including increases in ALP activity, calcium nodule formation, and expression levels

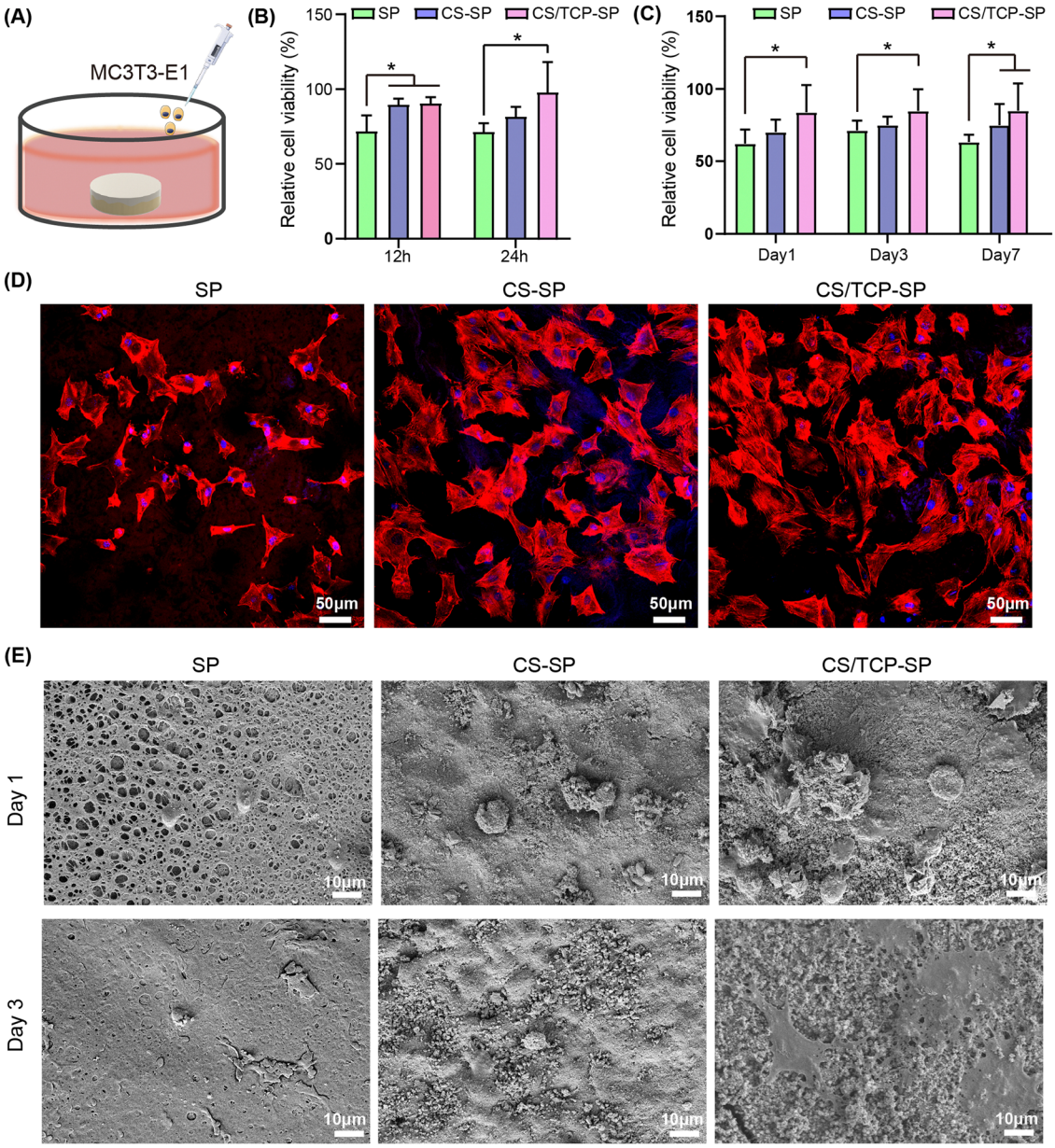

Fig. 3 Characterization of MC3T3-E1 responses to SP, CS–SP, and CS/TCP–SP surfaces: (A) experimental design of the MC3T3-E1 cells; (B) cell adhesion assessed by CCK-8 assay; (C) cell proliferation assessed by CCK-8 assay; (D) cell spreading observed by CLSM; and (E) cell morphology observed by SEM.

of osteogenic differentiation-related genes. β-TCP has been reported to be a good osteoinductive material with the capacity to degrade and release calcium and phosphorus ions to enhance osteoblast adhesion and osteogenic differentiation.[38] In contrast, CS was more osteoinductive with degrading and releasing Ca and Si ions to promote osteoblast adhesion, proliferation and osteogenic differentiation.[39]

3.5. *In vitro* osteo-immunomodulatory properties

Previous studies have focused predominantly on the impact of material properties on osteoblasts, with few investigations into the interactions of materials with immune and inflammatory cells. The focus of research and development in orthopedic biomaterials at present has shifted from the ability to promote osteogenesis to the ability to immunomodulate, particularly the ability to promote macrophage M2 polarization.[40] The adverse inflammatory and immunological reactions mediated by macrophages are among the main factors that are prone to lead to poor osseointegration of PEEK implants in the clinic.[41] Hence, endowing PEEK with immunomodulatory ability to avoid adverse immune responses has become a promising strategy to promote bone repair.

We cocultured different groups of materials with RAW264.7 cells and investigated the *in vitro* adhesion, proliferation, spreading and morphology of RAW264.7 cells, as well as the release of inflammatory factors and macrophage polarization to

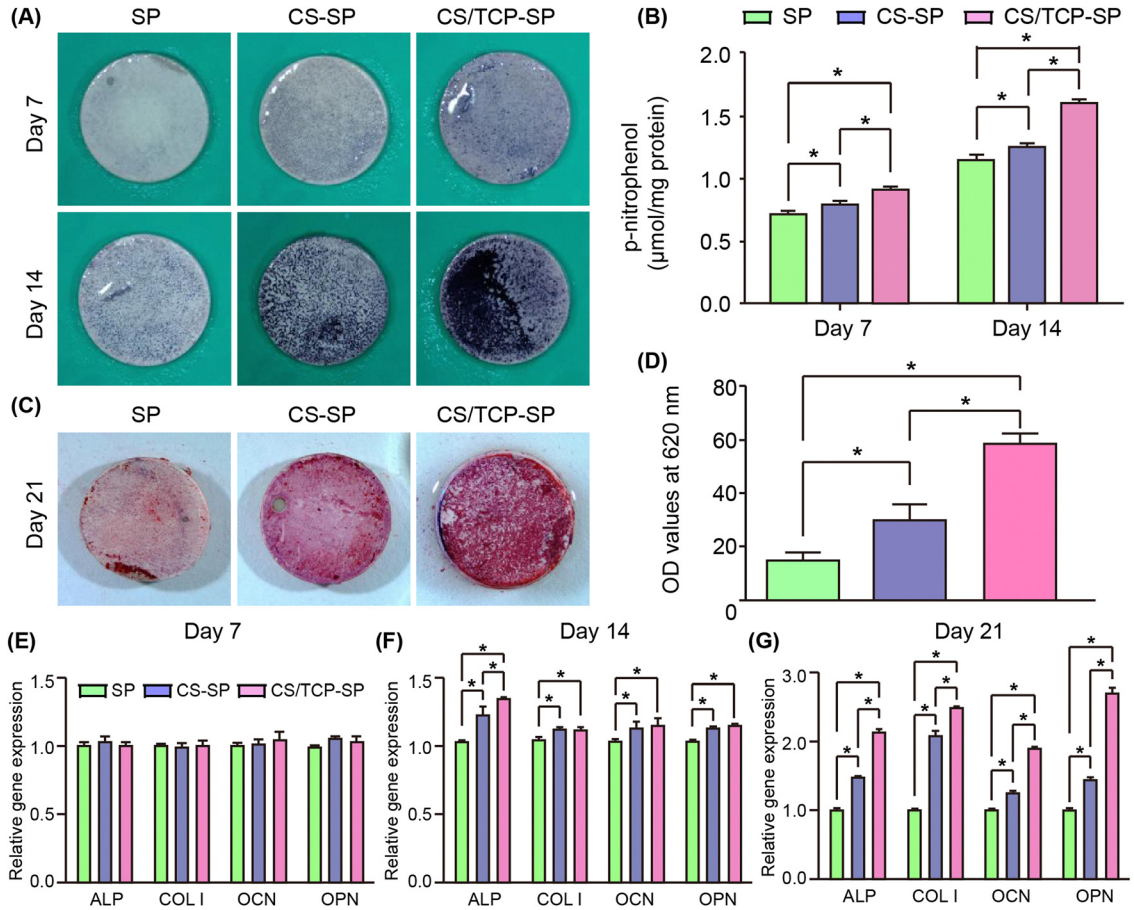

Fig. 4 Osteogenic differentiation of MC3T3-E1 cells on the SP, CS–SP, and CS/TCP–SP surfaces: (A) ALP staining; (B) quantitative analysis of ALP activity; (C) alizarin red staining; (D) quantitative analysis of calcium nodules; (E) expression of osteogenic differentiation-related genes at 7 days; (F) expression of osteogenic differentiation-related genes at 14 days; and (G) expression of osteogenic differentiation-related genes at 21 days.

assess the immunomodulatory capacity of the materials. In terms of cell adhesion, the CS–SP and CS/TCP–SP groups presented better cell adhesion than the SP group did at 6 hours (Fig. 5B). The proliferation of RAW264.7 cells in the three groups of materials was not significantly different, and the cell growth was satisfactory (Fig. 5C). SEM observations revealed that the RAW264.7 cells spread better on the CS–SP and CS/TCP–SP surfaces and possessed more pseudopods than on the SP surface did (Fig. 5D). These results demonstrated that the CS–SP and CS/TCP–SP coatings exhibited favorable cytocompatibility of macrophages.

Immune cells can secrete a variety of cytokines that directly affect the immune microenvironment, stem cell recruitment and osteogenic differentiation, which in turn affect bone regeneration and bone repair.[42] As shown in Fig. 5E–H, the CS–SP and CS/TCP–SP coatings secreted less TNF-α and IL-6 and more IL-4 and IL-10 from the RAW264.7 cells than did SP, and CS/TCP–SP secreted less TNF-α and more IL-4 from the RAW264.7 cells than did CS–SP.

Macrophage polarization, which can convert the macrophage phenotype into a proinflammatory M1 phenotype or an anti-inflammatory M2 phenotype, plays an extremely important role in bone immunomodulation.[43,44] CD206 is a surface marker of M2 macrophages, and iNOS is a surface marker of M1 macrophages. In our study, the immunofluorescence results (Fig. 5I–L) demonstrated that from SP to CS–SP and then to CS/TCP–SP, the fluorescence intensity of CD206 became progressively stronger, whereas the fluorescence intensity of iNOS became progressively weaker, and the quantitative analysis showed the same trend. These findings indicated that CS/TCP–SP and CS–SP promoted the M2 polarization of the macrophages, and CS/TCP–SP demonstrated a more pronounced effect.

Thus, the coated SP materials (CS–SP and CS/TCP–SP) promoted the adhesion and spreading of RAW264.7 cells, facilitated M1 to M2 polarization of the macrophages, and produced fewer proinflammatory factors (TNF-α and IL-6) and more anti-inflammatory factors (IL-4 and IL-10) than SP did; compared with CS–SP, CS/TCP–SP demonstrated a more pronounced immunoregulatory effect. Notably, there are several reasons for these results. Because CS/TCP–SP was more hydrophilic than CS–SP, the hydrophilic surface of the CS/TCP coating may enhance M2 polarization.[45] CS/TCP–SP may release phosphate ions compared with CS–SP. Phosphate ions have also been proved to induce increased differentiation toward the M2-anti-inflammatory macrophage phenotype.[46] Fukuda *et al.*

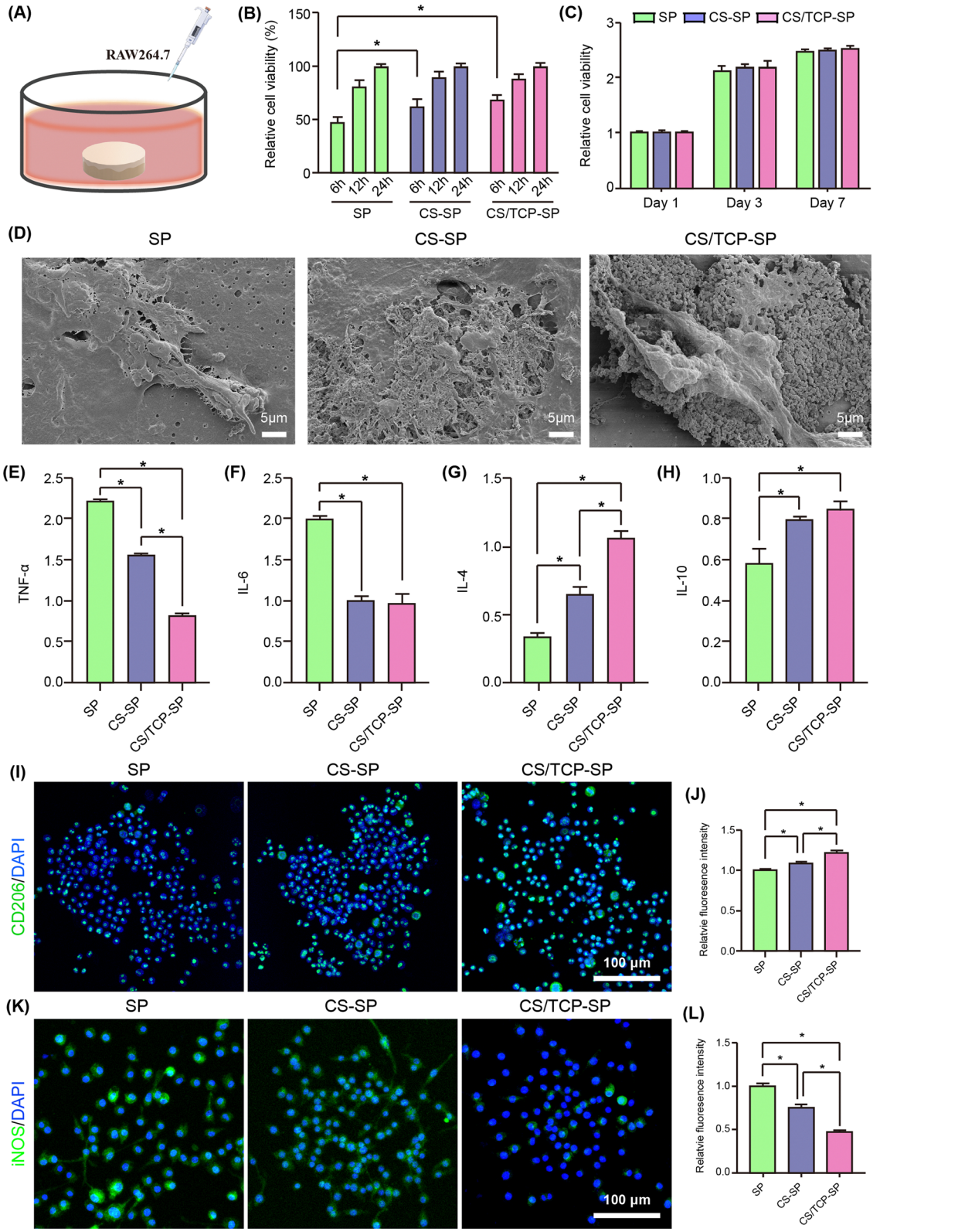

Fig. 5 Inflammatory response of RAW264.7 cells cultured on different samples: (A) experimental design of RAW264.7 cells; (B) cell adhesion assessed by the CCK-8 assay; (C) cell proliferation assessed by the CCK-8 assay; (D) cell morphology after culture for 24 hours; (E)–(H) secretion of (E) TNF-α, (F) IL-6, (G) IL-4, and (H) IL-10 after incubation for 3 days; (I) CD206 immunofluorescence staining at 3 days; (J) quantitative analysis of CD206 immunofluorescence staining; (K) iNOS immunofluorescence staining at 3 days; and (L) quantitative analysis of iNOS immunofluorescence staining.

reported that compared with bare and plasma-treated PEEK, phosphorylated PEEK could lower the levels of TNF-α but increase the levels of IL-10 produced by macrophages.[47] Compared with SP, CS–SP and CS/TCP–SP could release Ca and Si ions. The release of Ca ions from the coating materials was also a significant factor in the polarization of macrophages, especially during the M1 and M2 polarization of macrophages.[48,49] Similarly, Si ions promote macrophage polarization from the M1 phenotype to the M2 phenotype.[50]

3.6. Osteogenic differentiation of MC3T3-E1 cells in the conditioned medium

To determine the immunomodulatory effects of the modified samples on the osteogenesis of MC3T3-E1 cells, the conditioned medium from different samples seeded with macrophages was collected daily and supplied to MC3T3-E1 cells according to the protocols shown in Fig. 6A. The results of ALP staining and ALP activity quantitative analysis after conditioned culture revealed that the RAW264.7 (+)-conditioned media collected from CS/TCP–SP and CS–SP presented greater ALP activity of MC3T3-E1 cells than that from SP at both time points (Fig. 6B and C). In the CS/TCP–SP- or CS–SP-conditioned cultures, the intensity of alizarin red staining was also significantly greater than did the conditioned media collected from SP (Fig. 6D), which was consistent with the results of the quantitative analysis of alizarin red staining (Fig. 6E). In addition, the results of the quantitative analysis of alizarin red staining demonstrated that the number of calcium nodules formed by the cells after CS/TCP–SP-conditioned culture was slightly greater than that formed by the CS–SP-conditioned-cultured cells (Fig. 6E). Fig. 6F–I shows the expression of osteogenic differentiation-related genes of MC3T3-E1 cells after culture in RAW264.7 (+) conditioned medium collected from different samples at 7, 14 and 21 days. In general, the cells cultured in the CS/TCP–SP-conditioned medium exhibited significantly higher levels of COL I at 7 and 21 days, significantly higher levels of ALP at 14 and 21 days, significantly higher levels of OCN at 21 days and significantly higher levels of OPN at 14 and 21 days than did the cells cultured in the SP-conditioned medium, and the cells cultured in the CS–SP-conditioned medium exhibited significantly higher levels of COL I at 21 days, significantly higher levels of ALP at 14 and 21 days, and significantly higher levels of OCN at 7 and 21 days than did the cells cultured in the SP-conditioned medium. A comparison

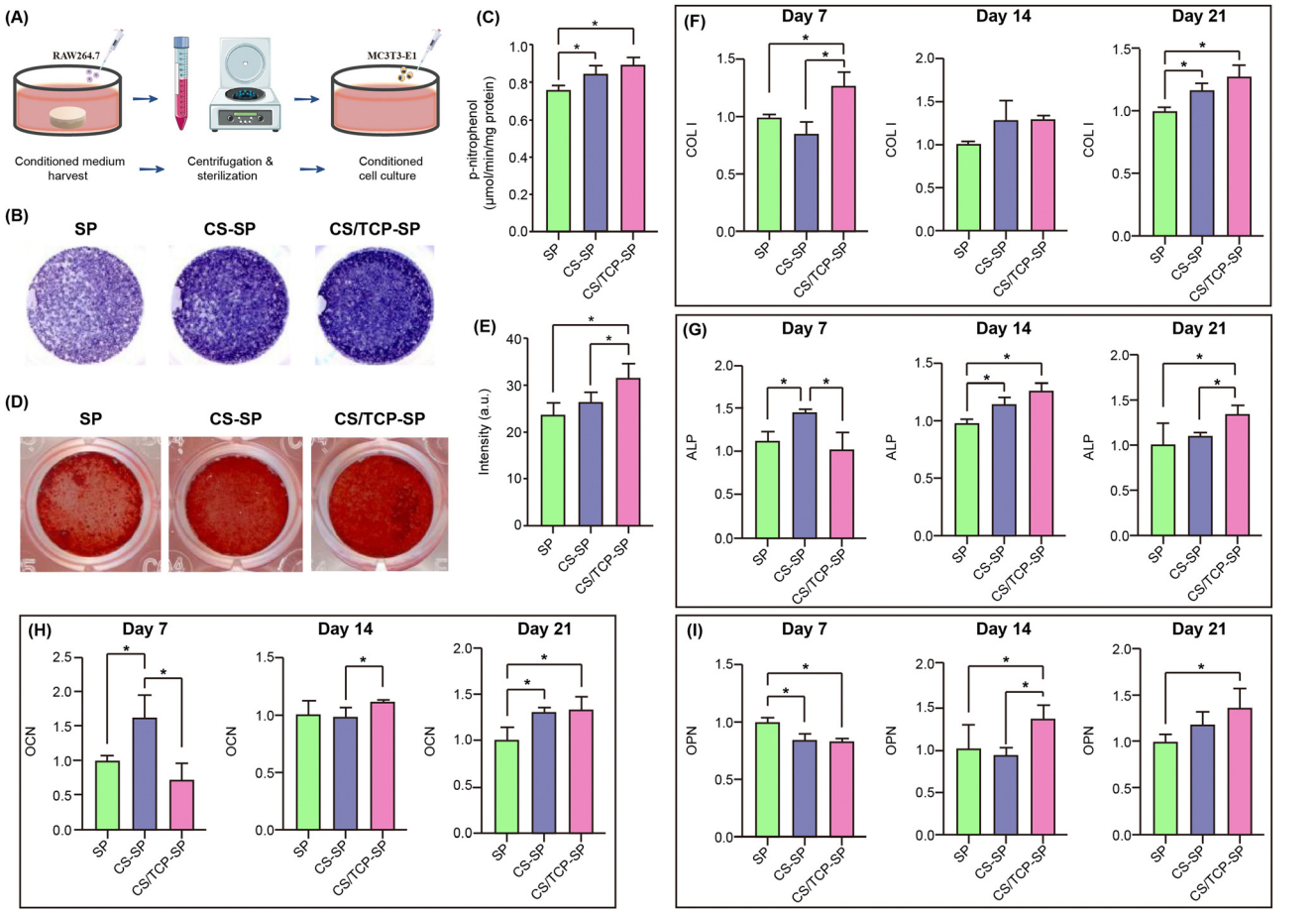

Fig. 6 Osteogenic differentiation of MC3T3-E1 cells in the conditioned medium: (A) experimental design of the conditioned culture and analysis; (B) ALP staining; (C) quantitative analysis of ALP activity; (D) alizarin red staining; (E) quantitative analysis of calcium nodules; (F) expression of the COL I gene; (G) expression of the ALP gene; (H) expression of the OCN gene; and (I) expression of the OPN gene.

of the cells cultured in CS/TCP–SP- and CS–SP-conditioned media revealed that the cells cultured in the CS/TCP–SP conditioned medium exhibited significantly higher levels of COL I at 7 days, significantly higher levels of ALP at 21 days, significantly higher levels of OCN at 14 days and significantly higher levels of OPN at 14 days than did the cells cultured under the CS–SP conditions.

Compared with SP and CS–SP, CS/TCP–SP promoted ALP expression and calcium nodule formation, as well as the expression of osteogenic differentiation-related genes. Concurrently, the capacity of CS/SP to facilitate osteogenic differentiation of surface cells was greater than that of SP. M2 macrophages secret cytokines to suppress initial inflammation while supporting osteogenic differentiation.[22,51] In this study, IL-4 and IL-10 secreted by RAW264.7 cells on the surface of the coated SP materials (CS–SP and CS/TCP–SP) positively affected the osteogenic differentiation of MC3T3-E1 cells. The Ca or Si ions released from the degradation of CS–SP and CS/TCP–SP could induce M2 macrophage polarization, cause the production of anti-inflammatory cytokines and promote osteogenic differentiation.[50,52] In addition to slower degradation, the advantage of CS/TCP–SP over CS–SP lies in the fact that β-TCP also has an immunomodulatory effect. β-TCP coating induced M2 macrophage phenotype polarization and significantly elevated the gene expression of the anti-inflammatory factor IL-1ra, thereby enhancing the osteogenic differentiation of BMSCs.[53]

3.7. Immunomodulatory evaluation *in vivo*

The implant triggers a "foreign body reaction" in the body, causes an acute inflammatory response and leads to activation of the M1 macrophages and subsequent secretion of large amounts of proinflammatory cytokines, such as IL-6, interleukin-1β (IL-1β), iNOS and TNF-α.[42,54] If the implant has no immunoregulatory capacity, M1 macrophages will continue to be activated, the acute inflammatory response will persist and progress to chronic inflammation, and fibrous connective tissue will form around the implant, encapsulating it and ultimately leading to failure of bone repair and osteointegration.[22] However, if the implant transitorily activates M1 macrophages and then polarizes to the M2 phenotype, thereby secreting anti-inflammatory cytokines, including arginine (Arg-1), IL-10, and IL-4, then an immunoregulatory microenvironment begins to form

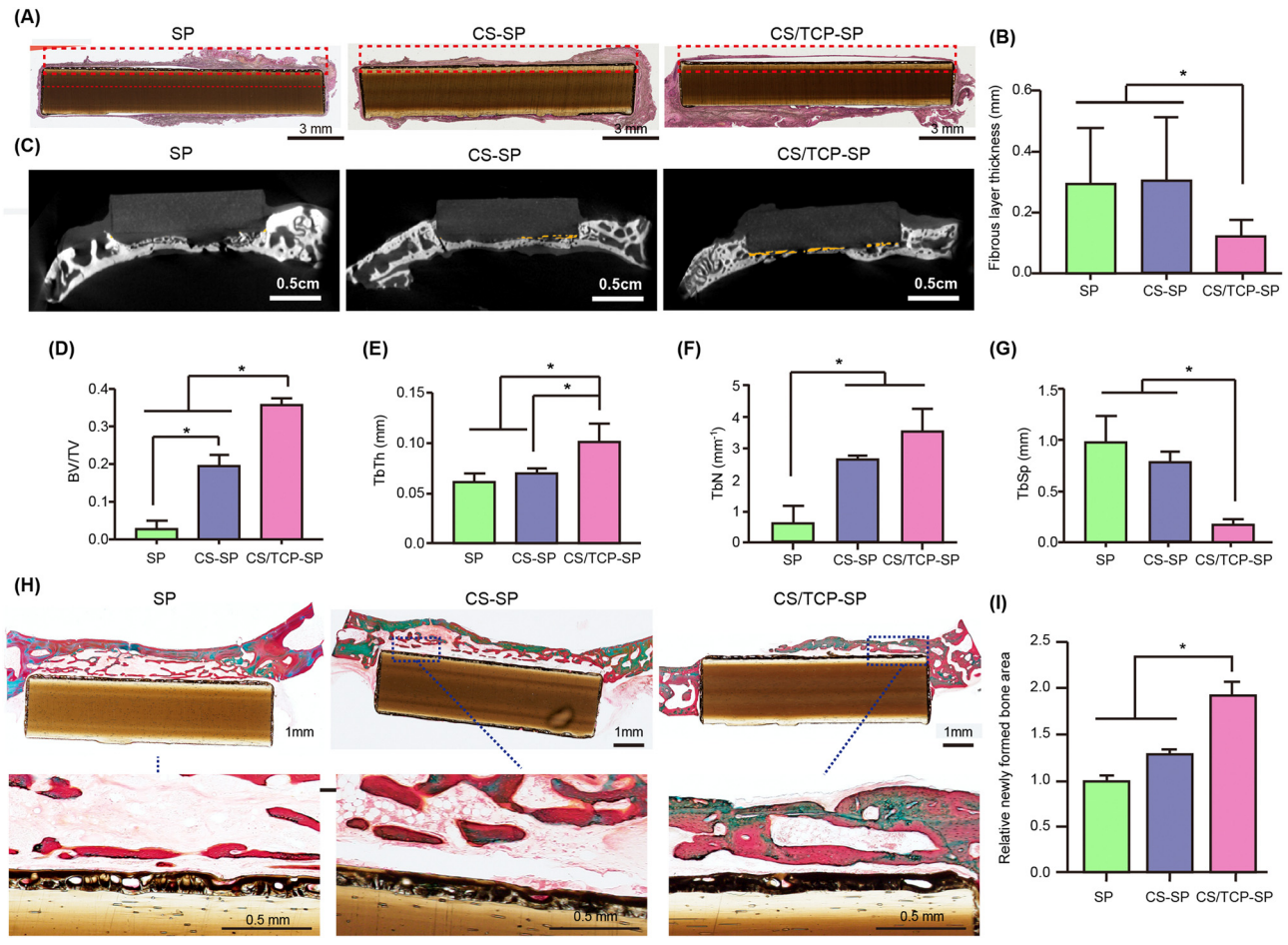

Fig. 7 *In vivo* immunomodulatory effects after 7 days and *in vivo* bone regeneration after 6 weeks: (A) H&E staining of the peri-implant tissues after subcutaneous implantation for 7 days; (B) thickness of the fibrous layers around the implants (n = 6 per group); (C) reconstructed coronal micro-CT images; (D)–(G) quantitative analysis of the micro-CT data including (D) BV/TV, (E) TBTh, (F) Tb·N and (G) Tb·Sp (n = 5 per group); (H) histological observation of the peri-implant tissues after Goldner staining; and (I) quantitative analysis of the newly formed bone area based on Goldner staining.

to promote bone repair and osteointegration at the bone–implant interface.[22] We established a rat air-pouch model and implanted the implants into a subcutaneous air-pouch. After 7 days, HE staining was performed to observe the thickness of the connective tissues around the implants, thereby evaluating the *in vivo* immunomodulatory ability of the materials. The thinner the connective tissue on the surface of the implant was, the more effectively it modulated the immune system.

The commonly used metal-based artificial joints can lead to the adsorption of proteins and the formation of wear particles when they are implanted in the body.[55] These alterations result in M1 macrophage polarization and the formation of a hyper-inflammatory microenvironment, which in turn causes fibrous tissue encapsulation and osteoclast activation and leads to aseptic prosthetic loosening.[22] In terms of both the qualitative (Fig. 7A) and quantitative results (Fig. 7B), the thickness of the fibrous connective tissue formed around the CS/TCP–SP was lower than those around SP and CS–SP. These findings indicated that CS/TCP–SP had a notable capacity to modulate the immune system *in vivo*. The fabrication of this immunomodulatory coating by vacuum cold spraying has the potential to be employed for surface modification of artificial joints. Compared with the hydrophobic surfaces, the hydrophilic surfaces can enhance the anti-inflammatory and pro-healing effects of macrophages.[56] This also applied to the hydrophilic CS/TCP–SP.

3.8. Bone-implant osseointegration *in vivo*

We established a rabbit cranial bone defect model and implanted different samples into the defect. The osteointegration and bone regeneration at the bone/implant interface were assessed by micro-CT and histological staining. Fig. 7C presents a coronal reconstruction image of the bone/implant interface around the implant. Correspondingly, the quantitative results of the osteogenesis-related parameters, including the BV/TV, TbTh, TbN, and TbSp, were analyzed and are shown in Fig. 7D–G. The results obtained from the CS/TCP–SP group were superior, followed by those of the CS–SP group, and those of the SP group were inferior. For the CS/TCP–SP sample, a higher BV/TV, TbTh and TbN implied more newly formed bones, and a lower TbSp implied denser newly formed bones, indicating that the quantity and quality of newly formed bones surrounding the CS/TCP–SP surface were significantly improved. Fig. 7F presents the results of Goldener staining. Similar to the results of the micro-CT, the newly formed bone surrounding the CS/TCP–SP was significantly thicker than those observed in the CS–SP and SP groups (Fig. 7H and I).

In conclusion, compared with the SP and CS-/SP materials, the CS/TCP–SP material exhibited superior osteointegration properties and was capable of promoting new bone formation at the bone/implant interface in comparison to those of the SP and CS/SP. The osteointegration of the CS/TCP–SP was significantly improved for several reasons. Firstly, changes in the surface properties (increased surface roughness and hydrophilicity) caused biological changes. Second, the apatite layer formed on the material surfaces was beneficial for osteointegration. Third, *n*-CS and β-TCP could degrade and release Ca and Si ions to promote bone regeneration. Fourth, the temporal regulation of M1 and M2 macrophages around the implant and the formation of an immunomodulatory microenvironment could facilitate the processes of osteogenic differentiation, osteointegration and bone regeneration around the implant.[22]

4. Conclusions

A biodegradable composite coating was prepared on the SP surface by vacuum cold spraying, and the 3D porous structure of the surface increased the bonding strength of the coating. The CS/β-TCP–SP material promoted osteoblast adhesion, proliferation, spreading and osteogenic differentiation *in vitro*, as well as osteointegration and bone regeneration *in vivo*. More importantly, the CS/TCP–SP stimulated the growth, spreading and M2 polarization of the macrophages, as well as the secretion of anti-inflammatory cytokines and exerted immunomodulatory effects to collectively facilitate the osteogenic differentiation of MC3T3-E1 cells. This biodegradable composite coating may be used as a biological PEEK joint prosthesis material.

Author contributions

Rui Ma: conceptualization, methodology, investigation, formal analysis, resources, visualization, writing – original draft, project administration, writing – reviewing and editing; Zidong Wu: methodology, investigation, formal analysis; Xiaoyu Guo: investigation, data curation, visualization; Zixuan Wu: methodology, investigation; Zheyue Zhu: methodology; Yuning Qu: methodology; Kunzheng Wang: resources, supervision; Chengxin Li: resources, project administration, supervision; Kai Ma: conceptualization, methodology, investigation, writing – original draft, project administration; and Pei Yang: funding acquisition, resources, project administration, supervision.

Data availability

The datasets generated and analyzed during this study are available in anonymized form to ensure reproducibility. Critical experimental parameters and characterization protocols have been thoroughly documented within the Experimental section. Computational models and analytical workflows are preserved following FAIR data principles (findable, accessible, interoperable, reusable). Researchers may request access to specific datasets through the corresponding author following institutional data sharing policies, subject to verification of academic purpose and confidentiality agreements where applicable. Processed data essential for interpreting the reported findings are fully incorporated into the manuscript figures and tables.

Conflicts of interest

There are no conflicts to declare.

Acknowledgements

Rui Ma, Kai Ma and Pei Yang designed the study. All authors reviewed the manuscript. This work was supported by the Fundamental Research Funds for the Central Universities (No. 11913224000029).

References

1 L. Fan, S. Chen, M. Yang, Y. Liu and J. Liu, *Adv. Healthcare Mater.*, 2024, **13**, e2302132.
2 S. Kumar, M. Nehra, D. Kedia, N. Dilbaghi, K. Tankeshwar and K. H. Kim, *Mater. Sci. Eng., C*, 2020, **106**, 110154.
3 R. Ma and T. Tang, *Int. J. Mol. Sci.*, 2014, **15**, 5426–5445.
4 R. Ma and D. Guo, *J. Orthop. Surg. Res.*, 2019, **14**, 32.
5 A. Gao, Q. Liao, L. Xie, G. Wang, W. Zhang, Y. Wu, P. Li, M. Guan, H. Pan, L. Tong, P. Chu and H. Wang, *Biomaterials*, 2020, **230**, 119642.
6 E. Buck, H. Li and M. Cerruti, *Macromol. Biosci.*, 2020, **20**, e1900271.
7 Z. Zheng, P. Liu, X. Zhang, X. Jingguo, W. Yongjie, X. Zou, X. Mei, S. Zhang and S. Zhang, *Mater. Today Bio*, 2022, **16**, 100402.
8 K. Ma, C. Li and C. Li, *J. Therm. Spray Technol.*, 2020, **30**, 571–583.
9 S. L. Zhang, Y. B. Shang, C. X. Li and C. J. Li, *Mater. Today Energy*, 2021, **21**, 100815.
10 J. Li, Y. Zhang, K. Ma, X. Pan, C. Li, G. Yang and C. Li, *J. Therm. Spray Technol.*, 2018, **27**, 471–482.
11 D. Li, Y. Gong, X. Chen, B. Zhang, H. Zhang, P. Jin and H. Li, *Surf. Coat. Technol.*, 2017, **330**, 87–91.
12 J. Lee, H. Jang, K. Lee, H. Baek, K. Jin, K. Hong, J. Noh and H. Lee, *Acta Biomater.*, 2013, **9**, 6177–6187.
13 J. Lee, H. Jang, K. Lee, H. Baek, K. Jin and J. Noh, *J. Biomed. Mater. Res., Part B*, 2017, **105**, 647–657.
14 R. Ma, J. Wang, C. Li, K. Ma, J. Wei, P. Yang, D. Guo, K. Wang and W. Wang, *J. Biomater. Appl.*, 2020, **35**, 342–352.
15 W. Gotz, E. Tobiasch, S. Witzleben and M. Schulze, *Pharmaceutics*, 2019, **11**, 117.
16 X. Liu, N. Zhao, H. Liang, B. Tan, F. Huang, H. Hu, Y. Chen, G. Wang, Z. Ling, C. Liu, Y. Miao, Y. Wang and X. Zou, *J. Orthop. Transl.*, 2022, **37**, 152–162.
17 S. Ni, J. Chang, L. Chou and W. Zhai, *J. Biomed. Mater. Res., Part B*, 2007, **80**, 174–183.
18 Y. Huang, X. Jin, X. Zhang, H. Sun, J. Tu, T. Tang, J. Chang and K. Dai, *Biomaterials*, 2009, **30**, 5041–5048.
19 M. Zakaria, A. Sulong, N. Muhamad, M. Raza and M. Ramli, *Mater. Sci. Eng., C*, 2019, **97**, 884–895.
20 M. Bohner, B. Santoni and N. Dobelin, *Acta Biomater.*, 2020, **113**, 23–41.
21 H. Wang, Y. Li, H. Li, X. Yan, Z. Jiang, L. Feng, W. Hu, Y. Fan, S. Lin and G. Li, *J. Orthop. Transl.*, 2025, **51**, 82–93.
22 N. Su, C. Villicana and F. Yang, *Biomaterials*, 2022, **286**, 121604.
23 M. Bosco, *J. Allergy Clin. Immunol.*, 2019, **143**, 1348–1350.
24 L. Xie, G. Wang, Y. Wu, Q. Liao, S. Mo, X. Ren, L. Tong, W. Zhang, M. Guan, H. Pan, P. K. Chu and H. Wang, *Innovation*, 2021, **2**, 100148.
25 Z. Chen, T. Klein, R. Murray, R. Crawford, J. Chang, C. Wu and Y. Xiao, *Mater. Today*, 2016, **19**, 304–321.
26 Y. Zhao, H. Wong, W. Wang, P. Li, Z. Xu, E. Chong, C. Yan, K. Yeung and P. Chu, *Biomaterials*, 2013, **34**, 9264–9277.
27 T. Kokubo, H. Kim and M. Kawashita, *Biomaterials*, 2003, **24**, 2161–2175.
28 F. Baino and S. Yamaguchi, *Biomimetics*, 2020, **5**, 57.
29 T. Kokubo and H. Takadama, *Biomaterials*, 2006, **27**, 2907–2915.
30 X. Liu, C. Ding and P. Chu, *Biomaterials*, 2004, **25**, 1755–1761.
31 G. Kaur, O. Pandey, K. Singh, D. Homa, B. Scott and G. Pickrell, *J. Biomed. Mater. Res., Part A*, 2014, **102A**, 254–274.
32 R. Ma, Y. Li, J. Wang, P. Yang, K. Wang and W. Wang, *J. Mater. Sci.: Mater. Med.*, 2020, **31**, 98.
33 K. Hotchkiss, G. Reddy, S. Hyzy, Z. Schwartz, B. Boyan and R. Olivares-Navarrete, *Acta Biomater.*, 2016, **31**, 425–434.
34 S. Guo, X. Zhu, M. Li, L. Shi, J. Ong, D. Janczewski and K. Neoh, *ACS Appl. Mater. Interfaces*, 2016, **8**, 30552–30563.
35 H. Fan and Z. Guo, *Biomater. Sci.*, 2020, **8**, 1502–1535.
36 R. Ma, Y. Su, R. Cao, K. Wang and P. Yang, *Int. J. Nanomed.*, 2023, **18**, 5055–5072.
37 S. Vermeulen, Z. Tahmasebi Birgani and P. Habibovic, *Biomaterials*, 2022, **283**, 121431.
38 J. Park, Y. Kim, J. Jang, T. Kwon, Y. Bae and J. Suh, *Acta Biomater.*, 2010, **6**, 1661–1670.
39 S. Ding, Y. Chu and P. Chen, *ACS Omega*, 2021, **6**, 7106–7118.
40 H. Chai, W. Wang, X. Yuan and C. Zhu, *Bioengineering*, 2022, **9**, 747.
41 X. Liu, L. Ouyang, L. Chen, Y. Qiao, X. Ma, G. Xu and X. Liu, *Regener. Biomater.*, 2022, **9**, rbab076.
42 Z. Julier, A. Park, P. Briquez and M. Martino, *Acta Biomater.*, 2017, **53**, 13–28.
43 D. Mosser and J. Edwards, *Nat. Rev. Immunol.*, 2008, **8**, 958–969.
44 S. Chow, C. Wong, C. Cui, M. Li, R. Wong and W. Cheung, *J. Orthop. Transl.*, 2022, **36**, 83–90.
45 Sunarso, A. Tsuchiya, N. Fukuda, R. Toita, K. Tsuru and K. Ishikawa, *J. Biomater. Sci., Polym. Ed.*, 2018, **29**, 1375–1388.
46 R. Villa-Bellosta, M. Hamczyk and V. Andres, *PLoS One*, 2017, **12**, e0174998.
47 N. Fukuda, A. Tsuchiya, Sunarso, R. Toita, K. Tsuru, Y. Mori and K. Ishikawa, *Colloids Surf., B*, 2019, **173**, 36–42.
48 E. Kelly, L. Wang and L. Ivashkiv, *J. Immunol.*, 2010, **184**, 5545–5552.
49 Z. Zhang, X. Zhang, Z. Zheng, J. Xin, S. Han, J. Qi, T. Zhang, Y. Wang and S. Zhang, *Mater. Today Bio*, 2023, **22**, 100748.
50 H. Li, W. Wang and J. Chang, *Regener. Biomater.*, 2021, **8**, rbab056.

51 B. Sinder, A. Pettit and L. McCauley, *J. Bone Miner. Res.*, 2015, **30**, 2140–2149.
52 R. Toita, Sunarso, A. Rashid, K. Tsuru and K. Ishikawa, *J. Mater. Chem. B*, 2015, **3**, 8738–8746.
53 Z. Chen, X. Mao, L. Tan, T. Friis, C. Wu, R. Crawford and Y. Xiao, *Biomaterials*, 2014, **35**, 8553–8565.
54 E. Ingham and J. Fisher, *Biomaterials*, 2005, **26**, 1271–1286.
55 R. Supra and D. K. Agrawal, *J. Orthop. Sports Med.*, 2023, **5**, 9–19.
56 L. Lv, Y. Xie, K. Li, T. Hu, X. Lu, Y. Cao and X. Zheng, *Adv. Healthcare Mater.*, 2018, **7**, e1800675.